BIOCHEMISTRY
including biophysical chemistry & molecular biology

ARTICLE

pubs.acs.org/biochemistry

Unfolding Distinguishes the *Vibrio cholerae* Cytolysin Precursor from the Mature Form of the Toxin

Karan Paul and Kausik Chattopadhyay*

Indian Institute of Science Education and Research (IISER) Mohali, Transit Campus: MGSIPAP Complex, Sector 26, Chandigarh 160019, India

Supporting Information

ABSTRACT: *Vibrio cholerae* cytolysin (VCC) is a potent cytolytic toxin that induces colloid osmotic lysis of its target eukaryotic cells by forming transmembrane oligomeric β-barrel channels. VCC is secreted by the bacteria as an inactive precursor (Pro-VCC) and is subsequently activated by proteolytic removal of an N-terminal "Pro-domain", thus generating the active form of the toxin (Mature-VCC). Earlier studies have indicated an intramolecular chaperone-like role of the Pro-domain favoring efficient secretion of the toxin from the periplasm into the extracellular space. However, the exact role of the Pro-domain in the VCC structure−function mechanism remains unclear. Here, we have compared the Pro-VCC and Mature-VCC molecules in terms of their structural and conformational properties. We have studied unfolding of the two variants of the VCC molecule in response to an array of denaturing conditions, including low-pH, chemical denaturant and heat-induced unfolding. Pro-VCC shows a more profound tendency to unfold in response to such denaturing conditions compared to Mature-VCC. Biophysical characterization of the isolated Pro-domain further suggests that the increased unfolding propensity of Pro-VCC does not arise because of an increased level of unfolding of the Pro-region itself. Altogether, our results imply that a natively folded architecture of the Pro-VCC molecule with sufficient structural and conformational plasticity presumably allows it to adopt a suitable configuration that is possibly required for its efficient secretion and subsequent proteolytic maturation under physiological conditions.

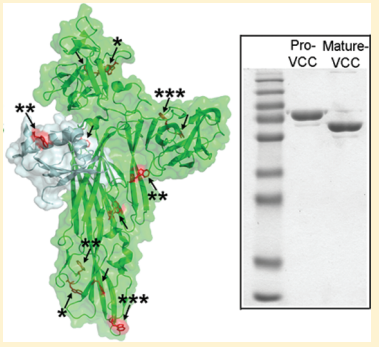

Bacterial β-barrel pore-forming toxins (β-PFTs) represent a special class of membrane-damaging cytolytic proteins that are implicated in a wide array of bacterial virulence mechanisms.[1,2] They are secreted by the bacteria as water-soluble monomers, and in contact with target cell membranes, they self-assemble to form transmembrane oligomeric β-barrel channels, thus destroying the natural permeability barrier function of the cell membranes.[3−6] Despite displaying this overall general scheme, β-PFTs differ significantly from each other in the intricate details of their mechanisms of action.[5] Unraveling the mechanistic details of the bacterial β-PFT mode of action is critically relevant in understanding the bacterial virulence mechanisms. Also, β-PFTs represent a unique class of dimorphic proteins that exist in two distinct conformational states: (a) the water-soluble monomeric state and (b) the transmembrane oligomeric assembly.[3−6] Such a unique dimorphic nature of the β-PFTs, in general, makes them suitable model systems for addressing numerous questions connected with the mechanisms of protein folding and unfolding pathways.[7]

Vibrio cholerae cytolysin (VCC) is a prominent member of the β-PFT family.[8] VCC is a potent membrane-damaging cytolytic protein toxin produced by most *V. cholerae* strains with high pathogenic and epidemic potential.[9−11] VCC is shown to induce lysis of a wide spectrum of eukaryotic cells.[12] Purified VCC causes the accumulation of fluid in ligated rabbit ileal loops, suggesting that the protein is potentially capable of contributing to the enteropathogenesis of cholera.[13] On the basis of these observations, VCC has been proposed as a potential virulence factor of *V. cholerae*.[1] The cytotoxic effects induced by VCC are attributed to its ability to form transmembrane oligomeric β-barrel channels in the target cell membrane; formation of transmembrane channels by VCC leads to colloid osmotic lysis of the target cells.[14−18]

The cytolytically active form of VCC is an ∼65 kDa molecule (Mature-VCC) that can oligomerize to form transmembrane heptameric pores in the target cell membranes.[19,20] However, the protein is synthesized in the bacteria as an ∼82 kDa molecule.[19] An N-terminal 25-residue signal peptide is cleaved off during the transport of the protein across the bacterial inner cell membrane, thus allowing extracellular secretion of the toxin as an ∼79.5 kDa inactive precursor called Pro-VCC. Conversion of Pro-VCC to the functionally active Mature-VCC requires proteolytic removal of an N-terminal, ∼14.5 kDa "Pro-domain" from Pro-VCC.[19] Such proteolytic activation of Pro-VCC can be achieved by the proteases present in the bacterial culture medium, and also in the target cell membranes.[21,22] The X-ray crystal structure of Pro-VCC has been determined at atomic resolution.[8] However, the high-resolution structure of Mature-VCC lacking the N-terminal Pro-domain is not available. Albeit, the Pro-VCC structure itself allows us to model the Mature-VCC structure. Comparison of

Received: March 4, 2011
Revised: April 13, 2011
Published: April 14, 2011

the entire Pro-VCC structure with the Mature-VCC part shows a similar surface hydrophobicity, but a somewhat distinct surface charge distribution (Figure S1 of the Supporting Information). Such analysis thus indicates an overall similar yet distinct structural architecture for the two proteins. Therefore, detailed experiments exploring structural comparison of Pro-VCC and Mature-VCC would be needed to conclusively establish whether proteolytic removal of the N-terminal Pro-domain would result in any major structural and/or conformational change(s) in the core domain(s) present in Mature-VCC.

The presence of the Pro-domain has been proposed to keep the toxin in a suitable state that allows the protein to be transported from the periplasmic space across the bacterial outer cell membrane into the extracellular medium.[23] Moreover, the presence of the Pro-domain keeps the toxin molecule in an inactive precursor state that is incapable of exerting the cytolytic activity toward its target cells.[19,23] It was also proposed that the Pro-domain could act as an intramolecular chaperone-like entity, thus influencing the structure, folding, and functional properties of the VCC toxin.[23] However, a detailed physicochemical treatment of such issues has not been pursued previously. Also, the exact requirement of the VCC toxin to be transported across the bacterial outer cell membrane as an inactive precursor, and not in its mature form, has not been addressed.

With the aim of gaining detailed insights into the role of the N-terminal Pro-domain in the VCC structure−function mechanism, in this work we have made an attempt to critically compare the physicochemical properties of the Pro-VCC and Mature-VCC molecules. We have studied the unfolding of the two variants of the VCC molecule in response to an array of denaturing conditions. Pro-VCC and Mature-VCC were subjected to low-pH, chemical denaturant, and heat-induced unfolding and were probed with respect to their structural and conformational changes. Pro-VCC displayed a more profound tendency to unfold in response to such denaturing conditions as compared to its mature counterpart, thus suggesting an increased structural plasticity of the precursor molecule in the presence of the Pro-domain. The isolated Pro-domain exhibited a markedly increased stability under similar denaturing conditions, thus suggesting that the increased level of unfolding of Pro-VCC arises not because of an increased unfolding propensity of the Pro-domain itself but rather because of long-range effect(s) induced on the mature part of the toxin in the presence of the Pro-domain. Our results imply that the presence of the Pro-domain distinguishes the Pro-VCC molecule from Mature-VCC by providing enough structural flexibility, thus probably making it more compatible with the transport machinery across the bacterial outer cell membrane.

EXPERIMENTAL PROCEDURES

Cloning, Expression, and Purification of Recombinant Pro-VCC and Mature-VCC. The nucleotide sequence encoding Pro-VCC (residues 26−741 of the full-length VCC precursor with an initial methionine) with an N-terminal AcTEV protease (Invitrogen) cleavage site was introduced into the pET-14b bacterial expression vector (Novagen). The pET-14b vector allows incorporation of an N-terminal six-His tag that facilitates initial purification of the protein using affinity chromatography on Ni-NTA agarose (Qiagen). The presence of the AcTEV protease site was useful for subsequent removal of the six-His tag.

Soluble Pro-VCC was expressed in *Escherichia coli* Origami B cells (Novagen) using the method described previously.[8] Briefly, *E. coli* Origami B cells harboring the cloned Pro-VCC gene in the pET-14b vector were grown in LB broth containing carbenicillin (50 μg/mL) at 37 °C to mid-log phase (A_{600} = 0.5). Protein expression was subsequently induced via growth at 30 °C for 3 h in the presence of 1 mM IPTG. Cells were harvested, resuspended in a buffer containing 20 mM sodium phosphate, 150 mM sodium chloride (pH 7.0) (PBS), and bacterial protease inhibitor cocktail (Sigma), and then lysed by ultrasonic disruption. The cell lysate was adjusted with 20 mM imidazole and passed through Ni-NTA agarose, and bound His-tagged protein was eluted with 300 mM imidazole in PBS. Eluted protein was exchanged with a buffer containing 10 mM Tris-HCl and 1 mM EDTA (pH 8.0) (buffer A) and loaded onto Q Sepharose Fast Flow (GE Healthcare/Amersham) resin. Bound protein was eluted with a linear gradient from 0 to 500 mM sodium chloride in buffer A. The N-terminal His tag was removed by treatment with AcTEV protease using the manufacturer's protocol followed by another round of purification by passing through Q Sepharose Fast Flow resin. Complete removal of the His tag was ensured by the absence of any detectable band in Western blotting using an anti-His antibody (Qiagen), in which an equivalent quantity of His-tagged Pro-VCC served as the positive control. Mature-VCC was generated from purified Pro-VCC via treatment with trypsin (at a protease:protein weight ratio of 1:2000) for 5 min at 25 °C. Mature-VCC was purified further when it was passed through Q Sepharose Fast Flow resin. Sodium dodecyl sulfate−polyacrylamide gel electrophoresis and Coomassie staining showed >98% purification of both the Pro-VCC and Mature-VCC proteins. Protein concentrations were determined by absorption at 280 nm on the basis of the theoretically calculated absorbance values (1.43 for 1 mg/mL Pro-VCC and 1.6 for 1 mg/mL Mature-VCC).

Hemolytic activities of Pro-VCC and Mature-VCC were measured against human erythrocytes (at 25 °C for 1 h) by determining the release of hemoglobin spectrophotometrically at 415 nm.[24,25] Consistent with the earlier reports,[19,23,24] the recombinantly generated Mature-VCC exhibited hemolytic activity against human erythrocytes, whereas recombinant Pro-VCC behaved as the cytolytically inactive precursor (data not shown).

Cloning, Expression, and Purification of the VCC Pro-Domain. The nucleotide sequence encoding the VCC Pro-domain (residues 26−127) was cloned into the pET-14b bacterial expression vector as described in the previous section. The VCC Pro-domain protein was expressed and purified following the method described above for Pro-VCC.

Fluorescence and Light Scattering Measurements. Fluorescence and light scattering measurements were taken using a Perkin-Elmer LS 55 spectrofluorimeter. Protein concentrations of 75 nM were used in all fluorescence and light scattering measurement experiments for Pro-VCC and Mature-VCC. A protein concentration of 1 μM was used in all fluorescence experiments for the VCC Pro-domain.

For intrinsic tryptophan fluorescence measurements, protein samples in a 1 cm path length cuvette were excited at 290 nm, with slit widths of 2.5 and 5.0 nm for excitation and emission, respectively. Each fluorescence emission spectrum was corrected for the baseline by subtraction of the appropriate buffer spectrum. For steady state tryptophan fluorescence intensity measurements, at least three data were collected at 340 and 355 nm, with an integration time of 20 s. All the intensity values were corrected for a suitable buffer blank.

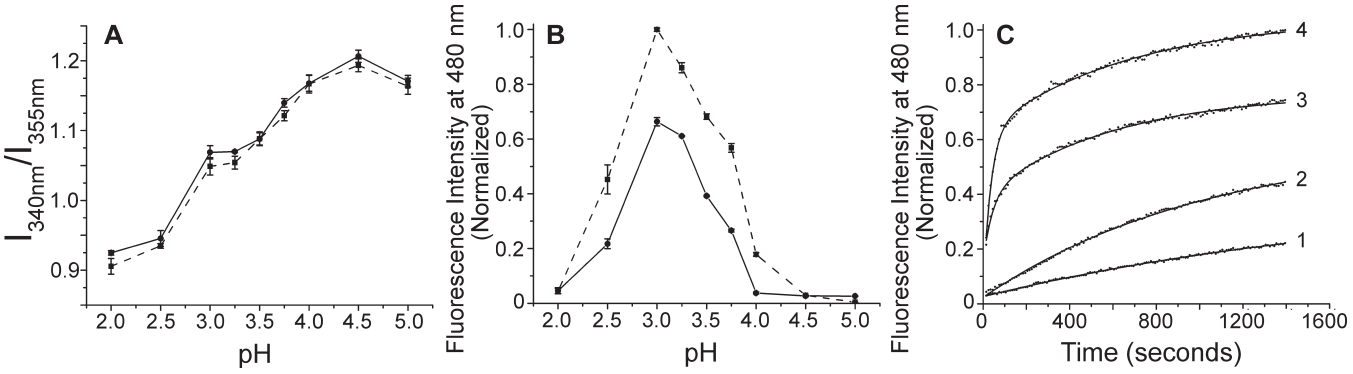

Figure 1. Low-pH-induced conformational changes in Pro-VCC and Mature-VCC as monitored by intrinsic tryptophan fluorescence and ANS binding. (A) Pro-VCC (---) and Mature-VCC (—) were incubated in 50 mM sodium citrate/citric acid buffer at the appropriate pH with 10 mM NaCl for 1 h at 25 °C, and intrinsic tryptophan fluorescence measurements were taken following the methods described in Experimental Procedures. The I_{340}/I_{355} values are plotted as a function of pH. Error bars indicate the standard deviations determined from at least three measurements. (B) Proteins were incubated at 25 °C in 50 mM sodium citrate/citric acid buffer at the appropriate pH with 10 mM NaCl. ANS fluorescence measurements were taken following the methods described in Experimental Procedures. Steady state ANS binding was monitored after incubation of the proteins for 1 h in the appropriate pH buffers. ANS fluorescence emission intensities were recorded at 480 nm for Pro-VCC (---) and Mature-VCC (—). Error bars indicate the standard deviations determined from at least three measurements. (C) Time courses of ANS binding monitored for Pro-VCC (curve 2, at pH 4.0; curve 4, at pH 3.0) and Mature-VCC (curve 1, at pH 4.0; curve 3, at pH 3.0). ANS binding kinetics were followed after the proteins were added to a given low-pH solution containing ANS. Data at pH 4.0 and 3.0 could be best fitted to single-exponential and biexponential functions, respectively. Solid lines through the data represent the exponential fits of the time course data.

Binding to hydrophobic dye 1-anilinonaphthalene-8-sulfonic acid (ANS) (Sigma) was monitored spectrofluorimetrically via excitation at 350 nm, with slit widths of 2.5 and 5.0 nm for excitation and emission, respectively. The final ANS concentration used was 2 μM. All the steady state ANS fluorescence measurements were taken at the 10 s time point after the addition of dye. For steady state ANS fluorescence intensity measurements, at least three data were collected at 480 nm, with an integration time of 20 s. All the intensity values were corrected for the suitable buffer blank containing ANS dye only. Kinetics of ANS binding were followed by monitoring the fluorescence intensity at 480 nm, at an interval of 10 s with integration time of 5 s.

Protein aggregation was monitored by recording the increase in light scattering at a right angle to the incident beam using the Perkin-Elmer LS 55 spectrofluorimeter setup. For studying the kinetics of aggregation, light scattering intensity values were recorded at 550 nm upon simultaneous excitation at the same wavelength, using slit widths of 2.5 and 2.5 nm for excitation and emission, respectively. Data were collected at an interval of 10 s with an integration time of 5 s.

Far-UV Circular Dichroism. Circular dichroism (CD) experiments were conducted on an Applied Photophysics Chirascan spectropolarimeter with a Peltier-based temperature controller using a 5 mm path length quartz cuvette. Protein concentrations in the range of 0.5−1 μM were used in all the far-UV CD experiments with Pro-VCC and Mature-VCC; 2−4 μM VCC Pro-domain was used for the far-UV CD experiments. Each spectrum was corrected for the baseline via subtraction of the appropriate buffer spectrum.

Analysis of Structures. The coordinates of the Pro-VCC crystal structure were obtained from the Protein Data Bank (PDB) (entry 1XEZ). The structural coordinates for the mature part of the VCC excluding the N-terminal Pro-domain were generated using PDBSET in the CCP4 suite.[26] Surface accessibility of tryptophan residues was calculated with areaimol[27] in the CCP4 suite.[26] All the structures were visualized using PyMOL [DeLano, W. L. (2002) *The PyMOL Molecular Graphics System*, found online (http://www.pymol.org)]. Surface electrostatic potentials on the structures were calculated and visualized using PyMol APBS tools.[28] Protein surface hydrophobic patches were estimated using the HOTPATCH server (http://hotpatch.mbi.ucla.edu/).

Data Analysis. OriginPro version 8.0 was used for data plotting and analysis. Nonlinear curve fitting functions available with OriginPro version 8.0 were used to analyze the steady state and kinetics data obtained from the fluorescence, light scattering, and CD measurements. In all cases, adjusted R^2 values as well as residuals were used to analyze the goodness of fit.

RESULTS

Low-pH-Induced Unfolding Triggers Similar Changes in the Global Tertiary Structures of Pro-VCC and Mature-VCC As Monitored by Intrinsic Tryptophan Fluorescence. In this study, the Pro-VCC molecule was recombinantly expressed and purified using a heterologous protein expression system in *E. coli*. The hemolytically active form of the protein, Mature-VCC, was generated from the precursor Pro-VCC by proteolytic removal of the N-terminal Pro-domain. The Pro-VCC and Mature-VCC molecules contain almost equivalent amounts of tryptophan residues [12 tryptophan residues (1.7%) in Pro-VCC and 11 tryptophan residues (1.9%) in Mature-VCC] (Figure S2 of the Supporting Information). Consistent with this, the two proteins displayed overall similar overlapping intrinsic tryptophan fluorescence emission profiles (upon excitation at 290 nm), both under native condition and under denaturing conditions (induced by 8 M urea) (data not shown).[24] This indicated possibly, but not necessarily (as the heterogeneity in the microenvironment of too many tryptophan residues may not be resolved), comparable tryptophan environments and, therefore, overall similar global tertiary structures for the precursor and the mature form of the VCC toxin.

To explore the possible differences in the physicochemical properties of Pro-VCC and Mature-VCC, we first studied the

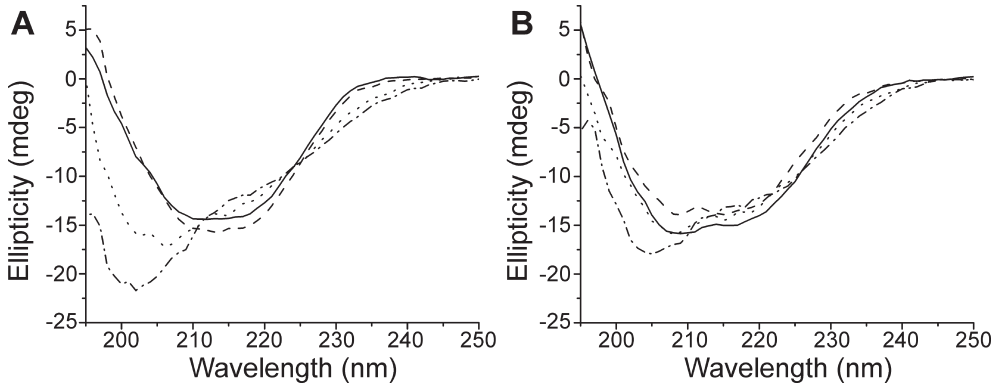

Figure 2. Low-pH-induced conformational changes in Pro-VCC and Mature-VCC as studied by far-UV CD. Far-UV CD spectra of Pro-VCC (A) and Mature-VCC (B) at pH 7.0 (—), 3.5 (---), 3.0 (· · ·), and 2.25 (—·—). Proteins were incubated at 25 °C for 30 min either in 5 mM Tris-HCl buffer (pH 7.0) with 5 mM NaCl or in 5 mM sodium citrate/citric acid buffer at the appropriate pH (3.5, 3.0, and 2.25) with 5 mM NaCl.

effect of low pH on the global tertiary structures of the two forms of the toxin molecule. We compared the intrinsic tryptophan fluorescence emission of the precursor and the mature protein as a function of different low-pH solution conditions to monitor the pH-induced unfolding behavior of the two proteins. A quantitative assessment of the low-pH-induced unfolding of Pro-VCC and Mature-VCC was conducted by monitoring the change in the variation in the fluorescence emission intensity pattern (I_{340}/I_{355}, the ratio of the fluorescence emission intensities at 340 and 355 nm), after excitation at 290 nm (Figure 1A). It is presumed that as the proteins would tend to unfold, there would be an increase in solvent exposure of the tryptophan residues, which in turn would result in a decrease in the I_{340}/I_{355} value. Both Pro-VCC and Mature-VCC exhibited similar and overlapping patterns in the change in the I_{340}/I_{355} values as a function of pH (Figure 1A). Up to pH 4.0, there was no substantial change in the I_{340}/I_{355} values. At pH <4.0, the I_{340}/I_{355} values changed steadily, showing marked alteration in the tryptophan microenvironments in both proteins, thus suggesting the changes in the global tertiary structures of both proteins. For both proteins, the changes in the I_{340}/I_{355} values as a function of pH showed a two-step transition in the unfolding pattern, one in the pH range of 3.0−4.0 and another in the pH range of 2.0−3.0. Altogether, the results clearly showed that both proteins, Pro-VCC and Mature-VCC, responded similarly to the acid-induced unfolding in the pH range of 2.0−4.0, in terms of their global tertiary structure changes.

Low-pH-Induced Unfolding Induces Different Extents of Local Conformational Changes in Pro-VCC and Mature-VCC As Revealed by ANS Binding. Next, we wanted to probe in further detail whether Pro-VCC and Mature-VCC could respond differently to low pH-induced unfolding in terms of any local conformational changes. Apart from the changes in global tertiary structures, low-pH conditions are known to induce local conformational changes in protein structures in terms of opening of exposed hydrophobic patches on the protein surfaces. Therefore, one attractive possibility was to explore the effect, if any, of different low-pH conditions in triggering exposure of hydrophobic patches on the protein surfaces of Pro-VCC and Mature-VCC. ANS is a hydrophobic dye that preferentially binds to exposed hydrophobic pockets on the protein surfaces that are rarely present in native folded proteins and are generally absent in fully unfolded proteins.[29,30] Consequently, the extent of ANS binding is considered as a measure of protein surface hydrophobicity. Binding of ANS to hydrophobic regions on protein surfaces leads to a marked increase in its fluorescence emission intensity, along with a significant blue shift in its fluorescence emission maximum (∼520 nm in water to 475−485 nm in a nonpolar environment). Exposure of Pro-VCC and Mature-VCC to the pH range of 3.0−4.0 resulted in a drastic increase in the ANS binding property (Figure 1B) of the two proteins. Interestingly, as compared to Mature-VCC, Pro-VCC displayed a much stronger tendency to bind to ANS starting from pH 4.0 (Figure 1B). Pro-VCC, but not Mature-VCC, showed considerable ANS binding even at pH 4.0, a solution condition that could not otherwise induce any major change in the global tertiary structure of the protein as revealed by our intrinsic tryptophan fluorescence studies (Figure 1A). Overall, our data suggested that the precursor protein generated more exposed hydrophobic patches on its surface during the low-pH-induced unfolding process. After further unfolding at pH <3.0, the ANS binding property decreased for both proteins. Consistent with the data depicted in Figure 1A, ANS binding appeared to be the property of the conformational states that existed only in the pH range of 3.0−4.0 for both Pro-VCC and Mature-VCC (Figure 1B). More pronounced unfolding below pH 3.0 [as monitored by changes in the I_{340}/I_{355} values for the intrinsic tryptophan fluorescence of Pro-VCC and Mature-VCC (Figure 1A)] could presumably abolish the specific pattern of hydrophobic patches responsible for binding to ANS.

After observing such a striking difference in the steady state ANS binding property of Pro-VCC and Mature-VCC, we also compared the kinetics of ANS binding for the two proteins, particularly at two pH values, pH 3.75 (the region in which both proteins started to exhibit moderate ANS binding) and pH 3.0 (the region in which both proteins exhibited maximal ANS binding) (Figure 1C). The kinetics of ANS binding at pH 3.75 could be fitted to a single-exponential function with time constants (t) of 9.6×10^{-4} and 5.26×10^{-4} s^{-1} for Pro-VCC and Mature-VCC, respectively. The kinetics of ANS binding at pH 3.00 could be best explained by a biexponential function with the following time constants: t_{fast} = 0.028 s^{-1} and t_{slow} = 0.0015 s^{-1} for Pro-VCC, and t_{fast} = 0.024 s^{-1} and t_{slow} = 0.00166 s^{-1} for Mature-VCC. At pH 3.00, Pro-VCC demonstrated a faster time constant for the "fast component" (t_{fast}), while the time constants for the "slow component" (t_{slow}) were similar for both proteins. Overall, under both pH conditions, the kinetics of binding of ANS to Pro-VCC were considerably faster

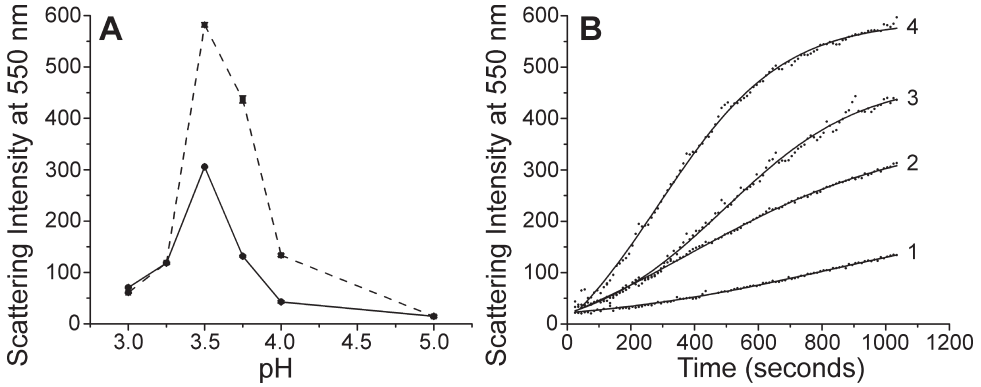

Figure 3. Low-pH-induced aggregation of Pro-VCC and Mature-VCC as monitored by the increase in light scattering intensity. Proteins were incubated at 25 °C in 50 mM sodium citrate/citric acid buffer at the appropriate pH with 10 mM NaCl. Protein aggregation was monitored by measuring the increase in light scattering intensity as discussed in Experimental Procedures. (A) Light scattering by Pro-VCC (---) and Mature-VCC (—) under different low-pH conditions. Scattering intensities were recorded ~10^3 s after incubation. Error bars indicate the standard deviations determined from at least three measurements. (B) Time courses of protein aggregation followed at two particular low-pH conditions for Pro-VCC (curve 3, at pH 3.75; curve 4, at pH 3.5) and Mature-VCC (curve 1, at pH 3.75; curve 2, at pH 3.5). Data could be best fit to a sigmoidal function as shown by solid lines.

than those of Mature-VCC. The kinetics of ANS binding could be directly correlated to the rate of local conformational change in the protein in terms of generation of surface-exposed hydrophobic patches on the protein. Therefore, our data showed that Pro-VCC responded to the low-pH conditions by undergoing local conformational change(s) at a much faster rate compared to that of Mature-VCC.

Changes in the Secondary Structure Elements during Low-pH-Induced Unfolding of Pro-VCC and Mature-VCC Distinguish the Precursor Protein from Its Mature Variant. The far-UV CD spectrum of Pro-VCC showed a broad negative minimum in the ellipticity values in the wavelength range of 209−218 nm (Figure 2A, solid line), characteristic of β-sheet rich proteins,[31] and such a spectrum corresponded well with the analysis of the crystal structure of the precursor protein.[8] Interestingly, conversion to the mature toxin resulted in a notable difference in the far-UV CD spectrum, showing a negative ellipticity minimum at 209 nm with a shoulder at ~218 nm (Figure 2B, solid line). Such dissimilarity between the overall shapes of the CD spectra for the two proteins indicated distinct differences in the secondary structure conformations of the two proteins. An accurate interpretation of the far-UV CD profile obtained here appears to be complicated as the far-UV CD spectra of β-sheet rich proteins are highly sensitive to the environment. Therefore, a high-resolution structural description of Mature-VCC would be required to more critically asses the detailed structural differences between the precursor and the mature toxin.

More striking differences between Pro-VCC and Mature-VCC were observed when the low-pH-induced secondary structural changes in the two proteins were monitored by recording the far-UV CD spectra under various low-pH conditions (Figure 2). For Mature-VCC in the pH range between 3.0 and 7.0, there was no major effect of the low-pH conditions on the far-UV CD spectra of the protein. At a more acidic pH of 2.25, however, there was a notable change in the CD spectrum, with a negative minimal peak of ellipticity at 205 nm, suggesting an increase in the amount of random coil structure in the protein (Figure 2B). Notably, the low-pH-induced alteration of the secondary structures was more profound in the case of Pro-VCC. Starting at pH 3.0, the far-UV CD spectra of Pro-VCC showed a negative minimal peak of ellipticity at ~205 nm. More severe secondary structure alteration was noticed for Pro-VCC at pH 2.25, for which the ellipticity minimum further shifted to 202 nm, with a significant increase in the negative ellipticity value (Figure 2A). These results clearly show that the two proteins, Pro-VCC and Mature-VCC, respond differently to low-pH-induced unfolding in terms of alteration of the secondary structure elements, with Pro-VCC being more susceptible to low-pH-induced structural alteration.

Pro-VCC and Mature-VCC Exhibit Different Extents of Aggregation during Low-pH-Induced Unfolding. As revealed by the ANS binding experiments, low-pH-induced unfolding of Pro-VCC and Mature-VCC in the pH range of 3.0−4.0 resulted in increased exposure of hydrophobic regions on the protein surfaces, with Pro-VCC being more susceptible to such an effect than its mature counterpart. It would, therefore, be an attractive hypothesis to test whether such increased exposure of surface hydrophobic patches would, in turn, result in an increased level of aggregation of the proteins. Aggregation of Pro-VCC and Mature-VCC induced by low pH was monitored by measuring light scattering from the protein solution. Because the intensity of light scattering at a given wavelength is proportional to the effective mass of the macromolecule, any increase in scattering intensity under low-pH conditions would signify a strengthened aggregation tendency of these two proteins. Both proteins displayed a significantly strengthened aggregation propensity at pH <4.0 (Figure 3A), with a maximal extent of aggregation being observed for both proteins at pH 3.5. The aggregation propensity was weakened below pH 3.5, and at pH 3.0, it nearly approached the minimal basal level. As revealed by our ANS binding data, exposure of surface hydrophobic patches on Pro-VCC and Mature-VCC was maximal at pH 3.0, which might, therefore, be expected to promote the chance of protein aggregation to the maximal extent. However, it should be emphasized that the increased level of protonation of the protein functional groups at an increased acidic pH would result in an increased and intermolecular charge repulsion, thus inhibiting the aggregation tendency of the protein molecules. Thus, the maximal aggregation of Pro-VCC and Mature-VCC at pH 3.5, and not at pH 3.0, could be considered as the result of an optimal compromise between the degrees of exposure of hydrophobic patches and the

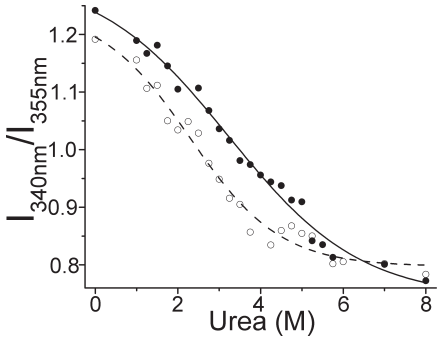

Figure 4. Urea-induced unfolding of Pro-VCC (○) and Mature-VCC (●) as monitored by intrinsic tryptophan emission fluorescence. The unfolding transition was monitored by changes in I_{340}/I_{355} as a function of urea concentration. Data were globally fit to a sigmoidal function to determine the apparent denaturant concentration at the midpoint of the curve [(---) fitting for Pro-VCC data and (—) fitting for Mature-VCC data]. All the experiments were conducted via incubation of the proteins at 25 °C for 1 h in 10 mM Tris-HCl buffer (pH 7.0) with 10 mM NaCl.

extent of net charge repulsion under the particular acidic condition. The kinetics of the protein aggregation process could be best fitted to a sigmoidal function for both proteins, with a transient lag phase followed by an extended exponential phase (Figure 3B). The presence of the transient lag phase prior to the exponential phase in the kinetics could be best explained by considering the possibility that the aggregation process preceded and was presumably triggered by the low-pH-induced exposure of the hydrophobic patches on the protein surfaces.

Consistent with the extent of exposure of surface hydrophobic patches during acid-induced unfolding, the precursor protein Pro-VCC also exhibited a markedly increased aggregation propensity as compared to that of its mature variant, Mature-VCC (Figure 3). The increased aggregation propensity of Pro-VCC at pH <4.0 could be directly attributed to the increased exposure of hydrophobic patches on the surface of Pro-VCC protein under the said pH conditions, as compared to its mature counterpart. The increased surface hydrophobicity of Pro-VCC could trigger aggregation of the protein even in the absence of any major alterations of its global tertiary structure, as observed from the combined protein tryptophan fluorescence (Figure 1A), ANS binding (Figure 1B,C), far-UV CD (Figure 2), and light scattering (Figure 3) data.

Chemical Denaturation at Physiological pH Reveals the Strengthened Unfolding Propensity of Pro-VCC Compared to That of Mature-VCC. So far, our data show that the Pro-VCC molecule was significantly more susceptible to low-pH-induced structural changes (in terms of exposure of hydrophobic patches on protein surface, alteration of secondary structure, and aggregation propensity) than the Mature-VCC protein. In this direction, we further explored the possibility of whether Pro-VCC responded differently compared to Mature-VCC to denaturing conditions even at physiological pH. We studied the urea-induced unfolding of Pro-VCC and Mature-VCC at pH 7.0 by monitoring the changes in the intrinsic tryptophan fluorescence (in terms of the I_{340}/I_{355} values) of the two proteins. The I_{340}/I_{355} values were plotted as a function of urea concentration (Figure 4). The data were globally fit to a two-state sigmoidal curve fitting function, and the midpoints of the transition from the native to the unfolded state were estimated. For Pro-VCC, the transition midpoint occurred in the urea concentration range of ∼2.25 M, whereas for Mature-VCC, the transition midpoint was found to be ∼3.25 M urea. It must be emphasized here that the fitting of the data was poor; therefore, the information obtained from such fitting should be considered only for qualitative purposes. This was possibly due to the fact that that the unfolding process did not follow the simple two-state native-to-denatured transition model. Earlier studies have shown that during urea-induced unfolding of Pro-VCC and Mature-VCC, formations of oligomeric species of the proteins are triggered in the moderately low denaturant concentration ranges.[24] Further studies would be needed to characterize such intermediate species formed during the unfolding process of the VCC proteins. Overall, in this study, the Pro-VCC protein exhibited a significantly strengthened tendency to respond to chemical denaturant-induced unfolding as compared to the Mature-VCC molecule, even at a physiological pH of 7.0.

Thermal Denaturation Triggers Differential Conformational Changes in Pro-VCC and Mature-VCC. To further establish the possible differences in the conformational stability of Pro-VCC and Mature-VCC, the effect of thermal denaturation on the structures of the two proteins was probed by far-UV CD spectroscopy. Changes in the far-UV CD profiles of the two proteins in the temperature range of 25−80 °C immediately showed a significant difference in the unfolding patterns of the two proteins (Figure 5A,B). To gain a more quantitative assessment of the structural and conformational change as a function of temperature, the ratios of the average ellipticity values in the wavelength range of 208−210 nm to those in the wavelength range of 217−219 nm ($mdeg_{@208-210nm}/mdeg_{@217-219nm}$) were plotted for the two proteins (Figure 5C). Such analysis, in combination with the overall pattern of the observed CD spectra, showed two-step conformational changes for both proteins during heat-induced denaturation. For Mature-VCC, over a temperature range starting at 50−55 °C, there was formation of unfolding intermediates with moderately altered secondary structure. At more elevated temperatures (>65 °C), the protein approached random coil structure. Pro-VCC exhibited a more drastic, two-stage conformational change: one starting at ∼45−50 °C inducing formation of a distinct intermediate with prominent red-shifted negative ellipticity minima at ∼218 nm and the next being triggered above 60 °C toward the random coil denatured state. As manifested in the far-UV CD profile, the effect of heat-induced unfolding on Pro-VCC structure and conformation was more profound in comparison to the effect on Mature-VCC, both qualitatively and quantitatively. These data, once again, suggested the notion that the precursor Pro-VCC displayed a considerably strengthened unfolding propensity compared to that of Mature-VCC.

Unfolding Behavior of the VCC Pro-Domain. So far, our study has indicated that the presence of the N-terminal Pro-domain considerably influenced the structural and conformational properties of the VCC molecule. In this direction, we further explored the possibility of whether the observed differential unfolding propensity of the Pro-VCC and Mature-VCC molecules arose because of the unfolding response within the Pro-domain only. For this, the physicochemical properties of the Pro-domain of the VCC protein were characterized in isolation. Analysis of the Pro-VCC crystal structure showed that the single tryptophan residue present in the Pro-domain was moderately exposed on the protein surface (Figure S2 of the Supporting Information) and was found to be consistent with the intrinsic tryptophan fluorescence emission profile of the Pro-domain (Figure 6A, inset). The far-UV CD spectrum of the Pro-domain

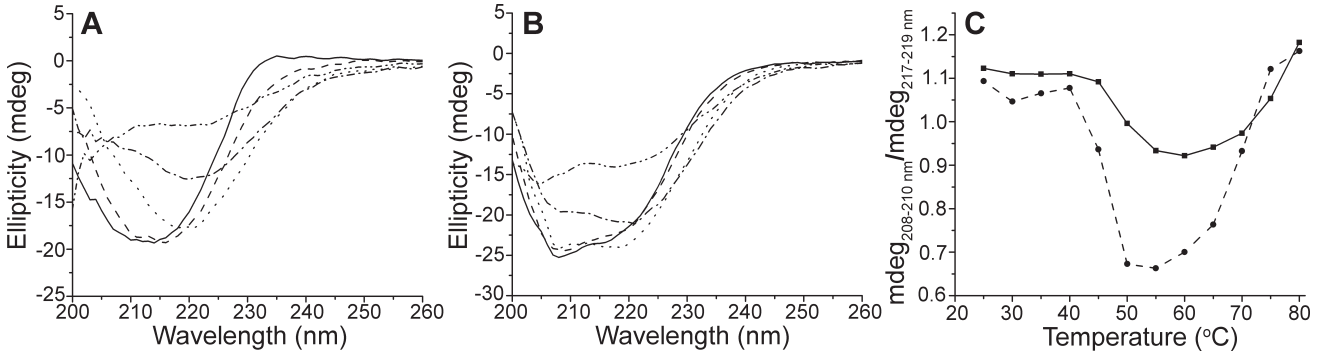

Figure 5. Thermal unfolding of Pro-VCC and Mature-VCC monitored by far-UV CD spectroscopy. Thermal unfolding reactions were conducted in 5 mM Tris-HCl buffer (pH 7.0) containing 5 mM NaCl via incubation of the proteins at a given temperature for 5 min. Panels A and B show the far-UV CD spectra of Pro-VCC and Mature-VCC, respectively, at 30 (—), 45 (---), 50 (· · ·), 65 (—·—), and 75 °C (—· · —). (C) Plot of $mdeg_{@208-210nm}/mdeg_{@217-219nm}$ at various temperatures in the range of 25−80 °C, displaying the changes in the secondary structure conformations of Pro-VCC (---) and mature-VCC (—) as a function of temperature.

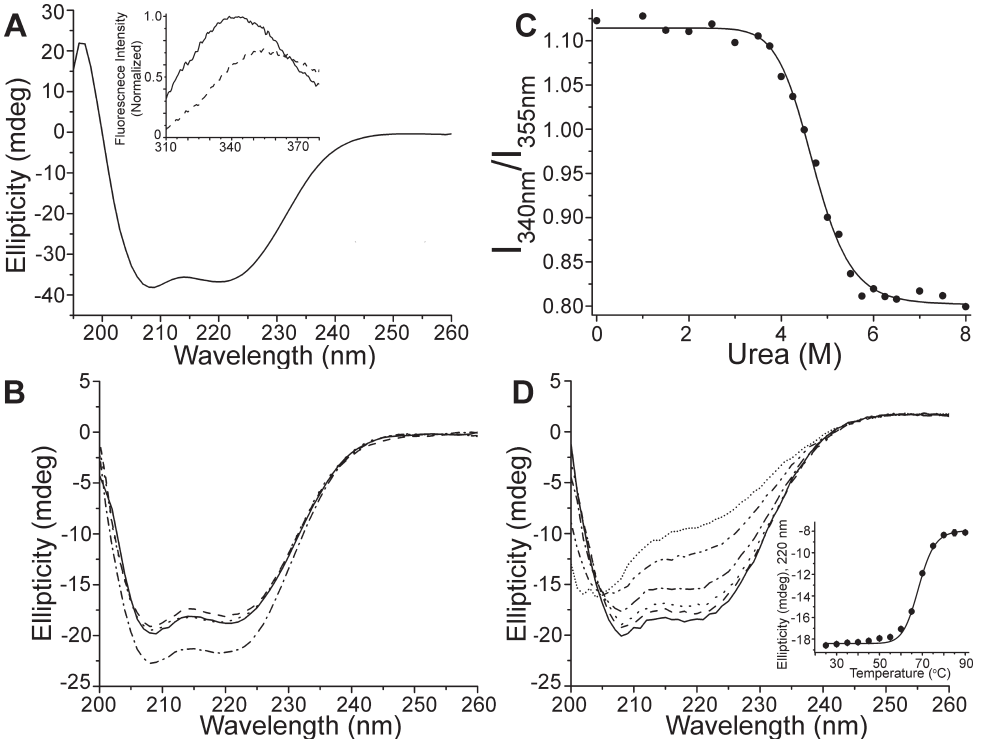

Figure 6. Characterization of the VCC Pro-domain. (A) Far-UV CD spectra of the Pro-domain protein in 5 mM Tris-HCl buffer (pH 7.0) containing 5 mM NaCl. The inset shows the intrinsic tryptophan fluorescence emission spectra of the Pro-domain in native and denatured states: (—) protein in 0 M urea and (---) protein in 8 M urea. Spectra were recorded in 10 mM Tris-HCl buffer (pH 7.0) containing 10 mM NaCl. (B) Far-UV CD spectra of the Pro-domain protein at pH 6.0 (—), 4 (---), 3.0 (· · ·), and 2.0 (—·—). Proteins were incubated at 25 °C for 30 min in 5 mM sodium citrate/citric acid buffer at the appropriate pH with 5 mM NaCl. (C) Urea-induced unfolding of the Pro-domain protein as monitored by intrinsic tryptophan emission fluorescence. The unfolding transition was monitored by changes in I_{340}/I_{355} values (●) as a function of urea concentration. Data were globally fit to a sigmoidal function to determine an apparent denaturant concentration at the midpoint of the transitions. The solid line shows fitting for the I_{340}/I_{355} data. All the experiments were conducted via incubation of the proteins at 25 °C for 1 h in 10 mM Tris-HCl buffer (pH 7.0) containing 10 mM NaCl. (D) Thermal unfolding of the Pro-domain monitored by far-UV CD spectroscopy. Thermal unfolding reactions were conducted in 5 mM Tris-HCl buffer (pH 7.0) containing 5 mM NaCl via incubation of the proteins at a given temperature for 5 min. The far-UV CD spectra of the Pro-domain are shown at 30 (—), 55 (---), 60 (· · ·), 65 (—·—), 70 (—· · —), and 75 °C (· · ·). The inset shows the changes in ellipticity at 220 nm as a function of temperature and reflects the heat-induced melting of the secondary structural features in the Pro-domain protein. The solid curve indicates the fitting of the data to a sigmoidal function.

protein revealed a pattern consistent with a typical α-helix rich protein[32] with negative ellipticity minima at 208 and 220 nm (Figure 6A). In significant contrast to Pro-VCC and Mature-VCC, the Pro-domain protein neither exhibited any detectable change in its intrinsic tryptophan fluorescence emission profile nor displayed any significant enhancement in ANS binding

dx.doi.org/10.1021/bi200332g |*Biochemistry* 2011, 50, 3936–3945

during its exposure to low-pH solution conditions (data not shown). A similar result was obtained when the conformational changes in the Pro-domain protein in response to low-pH conditions were probed using far-UV CD. Up to pH 3.0, there was no significant change in the secondary structure content of the Pro-domain protein. At a more acidic pH of 2.0, there appeared to be an increase in non-native α-helical structure content in the Pro-domain protein (Figure 6B). When subjected to chemical denaturant-triggered unfolding, the Pro-domain protein showed a markedly increased resistance to urea-induced unfolding with a transition midpoint at ~4.75 M urea (Figure 6C). Consistent with these results, the Pro-domain protein also showed markedly increased resistance to the thermal unfolding process. Thermal denaturation of the Pro-domain followed a simple two-state unfolding, from a native state to a random coil state, with a transition midpoint around 65−70 °C (Figure 6D). Altogether, the N-terminal Pro-domain in isolation displayed a markedly weakened unfolding propensity under an array of denaturing conditions and thus represented a stable robust component of the VCC molecular structure. It is therefore evident that a strengthened unfolding propensity observed with the VCC molecule in the presence of the Pro-domain cannot be explained by the unfolding process within the Pro-domain itself.

DISCUSSION

VCC is one of the few unique members of the β-PFT family that exhibits atypical domain architecture. The Pro-VCC crystal structure shows that apart from the core cytolysin domain, the protein harbors three additional domains that are not typically documented in the conventional β-PFTs: the N-terminal Pro-domain that is proteolytically removed in the course of maturation and two C-terminal lectin-like domains that may contribute to binding to receptor(s) or receptor-like molecules present on the biomembranes.[8] However, the exact role(s) of these additional domains in VCC structure−function has not been explored in great detail. In particular, the requirement of the N-terminal Pro-domain, which does not seem to contribute as a functional part of the mature toxin, still remains unclear. The only other prominent β-PFT members containing similar Pro-domains in the toxin precursor forms are aerolysin from *Aeromonas hydrophila*[33,34] and α-toxin from *Clostridium septicum*.[35] The exact structure−function correlation of such a Pro-domain in the context of the β-PFT mode of action is poorly understood. In this study, we have attempted to explore the role of the N-terminal Pro-domain present in the precursor form of the VCC molecule in terms of its overall structural and conformational properties.

Under native conditions, both Pro-VCC and Mature-VCC reveal similar tryptophan environments as determined by intrinsic tryptophan emission fluorescence profiles of the two proteins. However, the two variants display notable differences in their far-UV CD profiles. The secondary structure contribution of the Pro-domain alone can possibly give rise to the distinct far-UV CD profile of the precursor protein. Also, it is plausible to hypothesize that the presence of the N-terminal Pro-domain could globally affect the conformational state of the VCC protein. A high-resolution three-dimensional structure of Mature-VCC lacking the Pro-domain can only possibly resolve this ambiguity. However, such similar yet distinct structural and conformational features of Pro-VCC and Mature-VCC raise the possibility of whether the precursor and the mature forms display any dissimilarity in terms of their physicochemical properties that might be relevant in the context of the mode of action of the VCC toxin molecule. To explore this hypothesis, we have conducted a detailed comparison of the unfolding behavior of the two forms of the VCC toxin, the precursor Pro-VCC and its proteolytically processed active variant, Mature-VCC. We have monitored unfolding of the VCC variants induced by an array of denaturing conditions such as exposure to low pH, chemical denaturants, and high temperatures. During exposure to such denaturing conditions, the precursor Pro-VCC appears to be more susceptible to structural and conformational changes and unfolding than Mature-VCC.

Our data clearly indicate that the Pro-VCC molecular structure could be perturbed more readily than that of its mature counterpart. Such a structural plasticity of the Pro-VCC molecule possibly makes the precursor molecule a suitable intermediate during the transport of the VCC toxin from the bacterial periplasm to the extracellular space. Secretion of the VCC protein across the bacterial inner cell membrane is dependent on the presence of the N-terminal ~25-residue signal peptide.[19] The signal peptide is cleaved off during transport through inner cell membrane, generating the Pro-VCC molecule. Pro-VCC in the periplasmic environment appears to adopt its native structure and conformation. However, for being secreted outside the cell, Pro-VCC has to be transported across the outer cell membrane. Although the detailed description of the components needed for the specific transport of Pro-VCC is not available, the general consensus is that a number of periplasmic chaperones, as well as large protein complexes forming tunnel-like assemblies in the bacterial outer membrane, are involved in such transport processes.[36] It is presumptive to think that during transport from the periplasm to the extracellular space, Pro-VCC, although already natively folded, would be able to allow adjustment(s) in its structure and conformation to accommodate interactions with chaperones and transporters.[36] This study clearly shows that the Pro-VCC structure is more amenable to structural and conformational alteration depending on its physicochemical environment. The Pro-VCC structure is, therefore, better suited than its mature form to meet the above-mentioned criteria for its efficient transport. However, to support this hypothesis, future studies targeting the interactions of the Pro-VCC molecule with the components of the bacterial outer membrane transport apparatus would be required.

In summary, we have studied the impact of the Pro-domain on the unfolding behavior of the VCC toxin. Earlier studies of the refolding of Pro-VCC and Mature-VCC suggested an intramolecular chaperone-like role of the Pro-domain guiding proper refolding of the molecule.[23] In the absence of the Pro-domain, the VCC molecule tends to refold to an oligomeric species that lacks the cytolytic activity.[24] In this direction, this study provides further support for the notion that the N-terminal Pro-domain present in the precursor form of the VCC toxin critically regulates its structure, conformation, and unfolding. Our study establishes Pro-VCC as a natively folded precursor protein with sufficient structural flexibility to allow structural and conformational fine-tuning in the course of secretion, and maturation to its functionally active state.

ASSOCIATED CONTENT

Supporting Information. Analysis of Pro-VCC and Mature-VCC structural models. This material is available free of charge via the Internet at http://pubs.acs.org.

AUTHOR INFORMATION

Corresponding Author

*Indian Institute of Science Education and Research (IISER), Mohali, Transit Campus: MGSIPAP Complex, Sector 26, Chandigarh 160019, India. Telephone and fax: 91-0172-2791024. E-mail: kausik@iisermohali.ac.in.

Funding Sources

We thank IISER Mohali for financial support.

ACKNOWLEDGMENT

We thank Neha Jain of IISER Mohali for assistance with CD instrumentation. We thank Dr. Samrat Mukhopadhyay of IISER Mohali for critically reading the manuscript and insightful comments.

ABBREVIATIONS

PFT, pore-forming toxin; VCC, *V. cholerae* cytolysin; ANS, 1-anilinonaphthalene-8-sulfonic acid; CD, circular dichroism.

REFERENCES

(1) Alouf, J. E., and Popoff, M. R. (2006) *The Comprehensive Sourcebook of Bacterial Protein Toxins*, 3rd ed., Academic Press, New York.

(2) Iacovache, I., Bischofberger, M., and van der Goot, F. G. (2010) Structure and assembly of pore-forming proteins. *Curr. Opin. Struct. Biol. 20*, 241–246.

(3) Iacovache, I., van der Goot, F. G., and Pernot, L. (2008) Pore formation: An ancient yet complex form of attack. *Biochim. Biophys. Acta 1778*, 1611–1623.

(4) Gonzalez, M., Bischofberger, M., Pernot, L., van der Goot, F., and Frêche, B. (2008) Bacterial pore-forming toxins: The (w)hole story? *Cell. Mol. Life Sci. 65*, 493–507.

(5) Tilley, S. J., and Saibil, H. R. (2006) The mechanism of pore formation by bacterial toxins. *Curr. Opin. Struct. Biol. 16*, 230–236.

(6) Heuck, A. P., Tweten, R. K., and Johnson, A. E. (2001) β-Barrel pore-forming toxins: Intriguing dimorphic proteins. *Biochemistry 40*, 9065–9073.

(7) Hermoso, J. A., Mancheno, J. M., and Pebay-Peyroula, E. (2006) X-ray and neutron diffraction approaches to the structural analysis of protein lipid interactions. In *Protein-Lipid Interactions* (Mateo, C. R., Gomez, J., Villalain, J., and Gonzalez Ros, J. M., Eds.) 1st ed., pp 63−110, Springer, Berlin.

(8) Olson, R., and Gouaux, E. (2005) Crystal structure of the *Vibrio cholerae* cytolysin (VCC) pro-toxin and its assembly into a heptameric transmembrane pore. *J. Mol. Biol. 350*, 997–1016.

(9) Kaper, J. B., Morris, J. G., Jr., and Levine, M. M. (1995) Cholera. *Clin. Microbiol. Rev. 8*, 48–86.

(10) Honda, T., and Finkelstein, R. A. (1979) Purification and characterization of a hemolysin produced by *Vibrio cholerae* biotype El Tor: another toxic substance produced by cholera vibrios. *Infect. Immun. 26*, 1020–1027.

(11) Goldberg, S. L., and Murphy, J. R. (1984) Molecular cloning of the hemolysin determinant from *Vibrio cholerae* El Tor. *J. Bacteriol. 160*, 239–244.

(12) Yamamoto, K., Al-Omani, M., Honda, T., Takeda, Y., and Miwatani, T. (1984) Non-O1 *Vibrio cholerae* hemolysin: Purification, partial characterization, and immunological relatedness to El Tor hemolysin. *Infect. Immun. 45*, 192–196.

(13) Ichinose, Y., Yamamoto, K., Nakasone, N., Tanabe, M. J., Takeda, T., Miwatani, T., and Iwanaga, M. (1987) Enterotoxicity of El Tor-like hemolysin of non-O1 *Vibrio cholerae*. *Infect. Immun. 55*, 1090–1093.

(14) Krasilnikov, O. V., Muratkhodjaev, J. N., and Zitzer, A. O. (1992) The mode of action of *Vibrio cholerae* cytolysin. The influences on both erythrocytes and planar lipid bilayers. *Biochim. Biophys. Acta 1111*, 7–16.

(15) Zitzer, A., Walev, I., Palmer, M., and Bhakdi, S. (1995) Characterization of *Vibrio cholerae* El Tor cytolysin as an oligomerizing pore-forming toxin. *Med. Microbiol. Immunol. 184*, 37–44.

(16) Ikigai, H., Akatsuka, A., Tsujiyama, H., Nakae, T., and Shimamura, T. (1996) Mechanism of membrane damage by El Tor hemolysin of *Vibrio cholerae* O1. *Infect. Immun. 64*, 2968–2973.

(17) Menzl, K., Maier, E., Chakraborty, T., and Benz, R. (1996) HlyA hemolysin of *Vibrio cholerae* O1 biotype E1 Tor. Identification of the hemolytic complex and evidence for the formation of anion-selective ion-permeable channels. *Eur. J. Biochem. 240*, 646–654.

(18) Yuldasheva, L. N., Merzlyak, P. G., Zitzer, A. O., Rodrigues, C. G., Bhakdi, S., and Krasilnikov, O. V. (2001) Lumen geometry of ion channels formed by *Vibrio cholerae* EL Tor cytolysin elucidated by nonelectrolyte exclusion. *Biochim. Biophys. Acta 1512*, 53–63.

(19) Yamamoto, K., Ichinose, Y., Shinagawa, H., Makino, K., Nakata, A., Iwanaga, M., Honda, T., and Miwatani, T. (1990) Two-step processing for activation of the cytolysin/hemolysin of *Vibrio cholerae* O1 biotype El Tor: Nucleotide sequence of the structural gene (hlyA) and characterization of the processed products. *Infect. Immun. 58*, 4106–4116.

(20) He, Y., and Olson, R. (2010) Three-dimensional structure of the detergent-solubilized *Vibrio cholerae* cytolysin (VCC) heptamer by electron cryomicroscopy. *J. Struct. Biol. 169*, 6–13.

(21) Nagamune, K., Yamamoto, K., Naka, A., Matsuyama, J., Miwatani, T., and Honda, T. (1996) In vitro proteolytic processing and activation of the recombinant precursor of El Tor cytolysin/hemolysin (pro-HlyA) of *Vibrio cholerae* by soluble hemagglutinin/protease of *V. cholerae*, trypsin, and other proteases. *Infect. Immun. 64*, 4655–4658.

(22) Valeva, A., Walev, I., Weis, S., Boukhallouk, F., Wassenaar, T. M., Endres, K., Fahrenholz, F., Bhakdi, S., and Zitzer, A. (2004) A cellular metalloproteinase activates *Vibrio cholerae* pro-cytolysin. *J. Biol. Chem. 279*, 25143–25148.

(23) Nagamune, K., Yamamoto, K., and Honda, T. (1997) Intramolecular chaperone activity of the pro-region of *Vibrio cholerae* El Tor cytolysin. *J. Biol. Chem. 272*, 1338–1343.

(24) Chattopadhyay, K., and Banerjee, K. K. (2003) Unfolding of *Vibrio cholerae* hemolysin induces oligomerization of the toxin monomer. *J. Biol. Chem. 278*, 38470–38475.

(25) Chattopadhyay, K., Bhattacharyya, D., and Banerjee, K. K. (2002) *Vibrio cholerae* hemolysin. Implication of amphiphilicity and lipid-induced conformational change for its pore-forming activity. *Eur. J. Biochem. 269*, 4351–4358.

(26) Collaborative Computational Project, Number 4. (1994) The CCP4 suite: Programs for protein crystallography. *Acta Crystallogr. D50*, 760–763.

(27) Lee, B., and Richards, F. M. (1971) The interpretation of protein structures: Estimation of static accessibility. *J. Mol. Biol. 55*, 379–400.

(28) Baker, N. A., Sept, D., Joseph, S., Holst, M. J., and McCammon, J. A. (2001) Electrostatics of nanosystems: Application to microtubules and the ribosome. *Proc. Natl. Acad. Sci. U.S.A. 98*, 10037–10041.

(29) Semisotnov, G. V., Rodionova, N. A., Razgulyaev, O. I., Uversky, V. N., Gripas, A. F., and Gilmanshin, R. I. (1991) Study of the "molten globule" intermediate state in protein folding by a hydrophobic fluorescent probe. *Biopolymers 31*, 119–128.

(30) Stryer, L. (1965) The interaction of a naphthalene dye with apomyoglobin and apohemoglobin. A fluorescent probe of non-polar binding sites. *J. Mol. Biol. 13*, 482–495.

(31) Eisele, J. L., and Rosenbusch, J. P. (1990) In vitro folding and oligomerization of a membrane protein. Transition of bacterial porin from random coil to native conformation. *J. Biol. Chem. 265*, 10217–10220.

(32) van Holde, K. E., Johnson, W. C., and Ho, P. S. (2006) *Principles of Physical Biochemistry*, 2nd ed., Prentice Hall, Upper Saddle River, NJ.

(33) Hardie, K. R., Schulze, A., Parker, M. W., and Buckley, J. T. (1995) *Vibrio* spp. secrete proaerolysin as a folded dimer without the need for disulphide bond formation. *Mol. Microbiol. 17*, 1035–1044.

(34) Howard, S. P., and Buckley, J. T. (1985) Activation of the hole-forming toxin aerolysin by extracellular processing. *J. Bacteriol. 163*, 336–340.

(35) Ballard, J., Crabtree, J., Roe, B. A., and Tweten, R. K. (1995) The primary structure of *Clostridium septicum* α-toxin exhibits similarity with that of *Aeromonas hydrophila* aerolysin. *Infect. Immun. 63*, 340–344.

(36) Scott, M., and Sandkvist, M. (2006) Toxin secretion systems. In *The comprehensive sourcebook of bacterial protein toxins* (Alouf, J. E., and Popoff, M. R., Eds.) 3rd ed., pp 83−105, Academic Press, New York.